ISSN 1330-3651 (Print), ISSN 1848-6339 (Online) https://doi.org/10.17559/TV-20220309035350
Original scientific paper

Friction Stir Welding Experiments on AZ31B Alloy to Analyse Mechanical Properties and Optimize Process Variables by TOPSIS Method

Selvaraj MARAPPAN*, Lenin KASIRAJAN, Vijayanand SHANMUGAM

Abstract: The present work involves friction stir welding of AZ31B magnesium alloy plates by using copper as tool pin material. The friction stir welding input factors namely tool pin profile, tool rotational speed, tool feed and tool angle were varied to find their influence on the quality of the processed zone. For mechanical and micro structural study of the processed specimens, tensile test, hardness test and microscopy tests were carried out. The Taguchi's experimental combination of L_{18} mixed orthogonal array has been utilized for conducting experiments. ANOVA was utilized to evaluate the influence of each input factor on the response measures. TOPSIS, the multi-response optimization technique was applied to obtain the optimal setting for getting enhanced results. The experimental results of the optimum set provided a tensile strength of 206.35 MPa, Percentage elongation of 7.4% and Vickers hardness of 68 which are 88.2%, 52.9% and 79% of the corresponding property values of the base material respectively. Microstructural study revealed the refinement of grains in the processed zone. However the enhancement of properties is prevented by the occurrence of defects.

Keywords: AZ31B magnesium alloy; copper; friction stir welding; mechanical properties; microstructural study

1 INTRODUCTION

The transportation industries are continuously searching for light materials to fabricate various vehicular and other structural components with the objective of reducing the overall weight of the vehicle that would result in lesser fuel consumption. Aluminium/aluminium alloys are the most sought-after lighter materials. But in recent times, magnesium (Mg) alloys, with lighter density than aluminium are being explored for structural applications. Aircraft industry has utilized magnesium alloys extensively to make many light weighted structural components. Many automobile giants are using magnesium alloys in the place of aluminium or steel to manufacture components such as steering wheels, driving wheels, steering columns, gear boxes etc [1-3]. Though magnesium has good strength to weight ratio, its limitations include lesser resistance to wear and corrosion and being chemically reactive [4]. For joining metal alloys like magnesium alloys and aluminium alloys which are lighter in density and difficult to join by conventional methods, the Welding Institute of United Kingdom developed a technique called friction stir welding (FSW), as an innovative solid state joining method in which the base plates kept adjacent to each other are recast along the required joining line without melting [5]. The principle of friction stir welding provides increased plasticity, much refined grain size due to dynamic recrystallization along with enhanced properties [6]. It is a joining process done in solid state itself especially for light metals and alloys using a rotating tool pin that is inserted in a hole under axial pressure to travel along the edges of the plates or sheets to be joined and be fixed above a back plate for support [7]. The most critical elements that influence the shape and size of the plastic material flow are a tool and joint configurations [8-10]. The tool pin generates heat along the travel due to friction among the tool and the base material as a result of which the base plates plastically deform, mix and join together and solidify. The pin which contacts the adjacent and bottom areas provides heat to those parts whereas the shoulder portion of the tool being in full contact with the top surfaces of the plate generates significant amount of heat. It is also the shoulder portion which stops the plastically deformed material from flowing outside [11]. Friction stir processing technique that produces only low amount of heat is broadly employed [12-13]. Moreover, in FSW, the joint quality is influenced primarily by the factors like tool profile, tool speed, tool feed and angle of tilt [14]. Friction stir process could produce joints that are characterized by almost nil defects, less distortion, minimum cracks and refined grains [15]. There is a variety of magnesium alloys among which AZ31B has attracted the focus for structural applications due to its promising characteristics [16]. Cao et al [17]. experimentally made lap joint configuration of Mg AZ31B by FSW technique and also studied the welding input factors impact on joining of Mg AZ31B. The input factor such as traverse speed has a significant reason for formation of defects. Rozal Rose et.al. [18] systematically performed a microstructural analysis and tested a tensile property of FSWed AZ61A Mg alloy. From the analysis it has been found that axial force plays an important role for formation of finer grains, hardness and subsequently tensile properties. Rajakumar and Balasubramanian [19] analysed the inter relationship between fsw parameters like traverse speed, shoulder diameter, hardness of tool material, diameter of pin and tool rotational speed on hardness corrosion rate and tensile strength of the FSWed AA1100 Al alloy. Kadaganchi et al. [20] developed a numerical model using response surface technology (RSM) technique to evaluate the performance characteristics like yield strength, ultimate tensile strength and percentage elongation of FSWed AA2014-T6 material. M. Prasad and Kiran Kumar Namala [21] carried out parametric optimization of dissimilar FSW of AA5083 To AA6061 by considering input parameters like tool rotational speed, welding speed and angle of tilt of tool. Experiments are conducted using Taguchi L9 orthogonal array (OA). Sanjay Kumar et al. [22] suggested that Taguchi method combined with grey relational analysis (GRA) is useful for optimization of multiple responses that are more complex than single objective optimization. In this, the impact of input factors namely tool tilt angle, rotational speed, tool pin profile on response measures

such as percentage elongation and tensile strength were reported. It is understood from the literature that many researchers modeled and optimized the FSW input factors using various optimization methods to evaluate optimum combination of input factors for obtaining better results. While addressing multi-objective optimization several input factors and their interrelationship need to be considered. However, most of the research works used conventional methods for solving multi-objective optimization problem. As of now a few attempts are made by using Multiple-criteria decision-making (MCDM) method for solving multi-objective optimization problem. Therefore in this study an effort has been taken for solving multi-objective optimization of FSW of AZ 31B Magnesium alloy via Technique for order of preference by similarity to ideal solution (TOPSIS) approach.

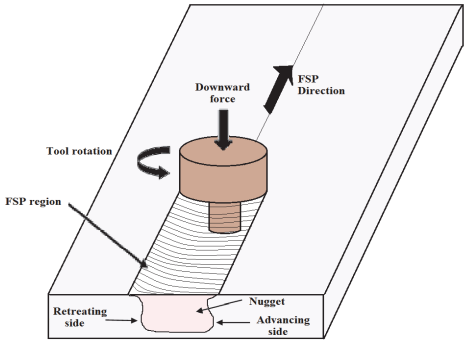

Figure 1 Friction stir welding (schematic)

Table 1 Various elements present in AZ31B Mg alloy (in wt. %)

Al	Zn	Mn	Si	Cu	Ca	Ni	Fe	Other	Mg
3.12	0.68	0.23	0.011	0.00021	0.031	0.0048	0.0003	0.19	Balance

Table 2 Properties of the AZ31B Mg alloy

Yield Strength / MPa	Ultimate Tensile Strength / MPa	Elongation in / %	Hardness / *HV*
124	234	14	86

2 WORK MATERIALS AND EXPERIMENTATION

In this study, the friction stir welding has been done on AZ31B Mg alloy plates of 100 × 100 × 6 mm dimensions. Tab. 1 lists the chemical elements found in the alloy, while Tab. 2 lists the Mg alloy's mechanical properties.

Table 3 FSW parameters and their levels

Parameters	Symbol	Level 1	Level 2	Level 3
Tool Pin Profile	P	Square	Threaded cylindrical	-
Tool Rotational Speed / RPM	N	1250	1350	1450
Welding Speed / mm/min	F	25	35	45
Tool Angle / °	θ	1	1.5	2

The FSW process has been done by using computer numerical controlled vertical machining center (VMC Make: Falcon Tools, Coimbatore, Tamilnadu, India), by developing a unique work holding device for clamping the work material. The tool pin dimensions include a shoulder of 18 mm diameter and 100 mm length and the pin having 5 mm length with 3.8 mm diameter for threaded cylinder and for square side as well. Tool pins profiles with two different geometries, one square pin and another threaded pin have been used in this investigation.

The tool was made of copper and tool pin profiles are presented in Fig. 2a and Fig. 2b. Four major input parameters each at three levels were utilized in accordance with Taguchi's experimental design of L18 mixed level for carrying out the trials. The input parameters investigated along with their levels are provided in Tab. 3.

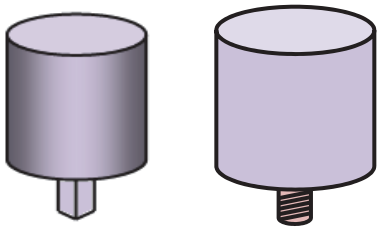

Figure 2 Schematic representation of the copper tool pins: a) square pin, b) threaded tool pin profile

2.1 Samples for Mechanical Testing

The samples were cut for required dimensions for using in tensile and hardness tests from the processed bulk using wire cut machine. The samples were properly polished and etched for taking micrographs. The tensile test specimen was cut from the FSW welded plates normal to joining line for dimensions in accordance with ASTM-E8 specification utilizing wire-cut EDM machine [23] as presented in Fig. 3a and Fig. 3b. The Universal Tensile Testing Machine (*UTS*) (MTS Insight: Electromechanical type with 100 KN, Standard length) was used to perform the tensile tests. The tensile tests were used to determine the tensile strength of the welded joint and also to measure the percentage elongation. The micro hardness of the processed region has been estimated by utilizing Vicker's micro hardness testing machine (Company: Sumitra Enterprises of New Delhi).

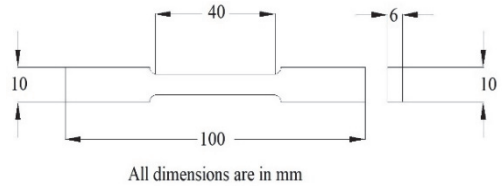

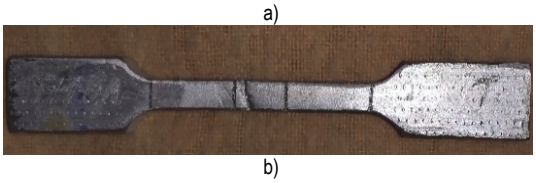

b)

Figure 3 (a) Tensile test specimen dimensions, (b) Tensile test specimen

Figure 4 Vickers Hardness test specimen

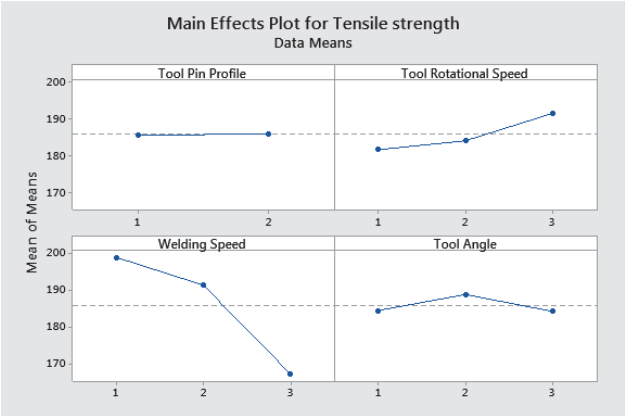

Figure 5 Main effects plot for tensile strength

For each specimen, micro hardness values were estimated at three distinct locations and as well as the mean value were utilized as final value.

3 RESULTS AND DISCUSSION

3.1 Impact of Parameters on Tensile Strength

The experimental results are presented in Tab. 4. The mean response table attained from Taguchi technique is often used to measure the impact on performance characteristics of each level of welding parameter. As the experiments are conducted based on the Taguchi's orthogonal array, it is easy to evaluate the influence of the welding input factor on the performance characteristics.

Table 4 Experimental conditions for FSW and test results of FS Welded samples

Exp. NO	Tool Pin Profile, *P*	Tool Rotational Speed, *N* / RPM	Welding Speed, *F* / mm/min	Tool Angle, θ / degree	*UTS* / MPa	% of Elongation	Avg *HV*
1	Square	1250	25	1	181.5	6.9	64
2	Square	1250	35	1.5	188.25	6.1	58
3	Square	1250	45	2	162.65	5.4	55
4	Square	1350	25	1	203.45	7.1	68
5	Square	1350	35	1.5	195.25	6.6	63
6	Square	1350	45	2	158.25	4.6	57
7	Square	1450	25	1.5	199.25	7.3	68
8	Square	1450	35	2	194.52	6.4	63
9	Square	1450	45	1	186.35	5.5	58
10	Threaded Cylindrical	1250	25	2	196.25	6.8	65
11	Threaded Cylindrical	1250	35	1	187.3	6	59
12	Threaded Cylindrical	1250	45	1.5	173.75	4.4	54
13	Threaded Cylindrical	1350	25	1.5	206.35	7.4	68
14	Threaded Cylindrical	1350	35	2	187.65	6.1	64
15	Threaded Cylindrical	1350	45	1	153.35	5.2	56
16	Threaded Cylindrical	1450	25	2	205.45	7.1	69
17	Threaded Cylindrical	1450	35	1	194.25	7.1	63
18	Threaded Cylindrical	1450	45	1.5	169.35	5.5	56

Table 5 Response table for the Tensile strength

Level	Tool Pin Profile , *P*	Tool Rotational Speed, *N* / RPM	Welding Speed, *F* / mm/min	Tool Angle, θ / degree
1	185.5	181.6	198.7	184.4
2	186.0	184.0	191.2	188.7
3	--	191.5	167.3	184.1
Delta	0.5	9.9	31.4	4.6
Rank	4	2	1	3

The mean value of tensile strength for all the welding parameters at each level is estimated and the results are given in Tab. 5. Based on the results it is found that factor *C* (Welding Speed) has the strongest effect on the tensile strength owed by factor *B* (Tool Rotational Speed) and factor *D* (Tool Angle). The Tool Pin Profile has the least effect on the tensile strength. The mean response plot of Tensile strength is presented in Fig. 5. The significance amongst the welding factors for output responses must also be calculated more precisely by using ANOVA analysis. The results of ANOVA analysis are given in Tab. 8. In this analysis, the consistency of process performance is recognized by greater R^2 Value. Anticipated R^2 and Adjusted R^2 shows more accurate results. On the basis of ANOVA results, the estimated R^2 value of *UTS* is R^2 = 95.55%. The R^2 values show that the experiment sequence has a high degree of confidence in the system, with a 90% significance level. It shows that welding speed (feed) is the most dominating factor of the process, showing an influence of 72.77% on *UTS*.

3.2 Impact of Parameters on Percentage Elongation

The experimental results are presented in Tab. 5. The mean response table attained from Taguchi technique is often used to measure the impact on performance characteristics of each level of welding parameter. As the experiments are conducted based on the Taguchi's orthogonal array, it is easy to evaluate the influence of all welding input factors on the performance characteristics. The mean value of percentage Elongation for all the welding parameters at each level is estimated and the results are given in Tab. 6. Based on the results it is found that factor *C* (Welding Speed) has the strongest effect on the percentage Elongation owed by factor *B* (Tool Rotational Speed) and factor *D* (Tool Angle). The Tool Pin Profile has the least effect on the percentage Elongation. The mean response plot of percentage Elongation is presented in Fig. 6. The significance amongst the welding factors for output responses must also be calculated more prcisely by using ANOVA analysis. The results of ANOVA analysis are given in Tab. 8. In this analysis, the consistency of process performance is recognized by greater R^2 value. Anticipated R^2 and Adjusted R^2 show more accurate results. On the Basis of ANOVA results, the estimated R^2 value of *POE*, R^2 = 97.11%. The R^2 values show that the experiment sequence has a high degree of confidence in the system, with a 90% significance level. It shows that welding speed (feed) is the most dominating factor of the process, showing an influence of 84.33% on *POE*.

Table 6 Response table for the percentage elongation

Level	Tool Pin Profile, *P*	Tool Rotational Speed, *N* / RPM	Welding Speed, *F* / mm/min	Tool Angle, θ / degree
1	6.211	5.933	7.100	6.300
2	6.178	6.167	6.383	6.217
3	--	6.483	5.100	6.067
Delta	0.033	0.550	2.000	0.233
Rank	4	2	1	3

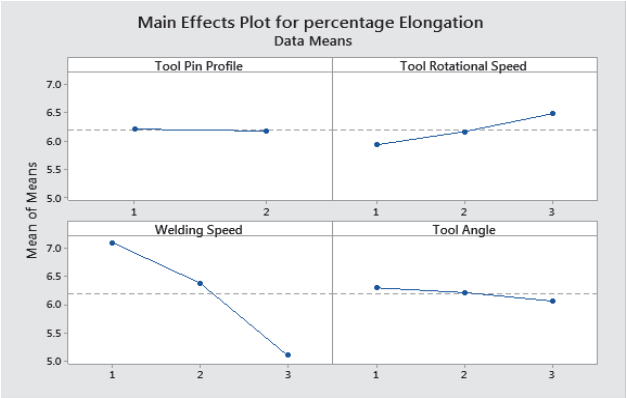

Figure 6 Main effects plot forpercentage elongation

3.3 Impact of Parameters on Hardness

The experimental results are presented in Tab. 5. The mean response table attained from Taguchi technique is often used to measure the impact on performance characteristics of each level of welding parameter. As the experiments are conducted based on the Taguchi's orthogonal array, it is easy to evaluate the influence of all welding input factors on the performance characteristics. The mean value of hardness for all the welding parameters at each level is estimated and the results are given in Tab. 7. Based on the results it is found that factor *C* (Welding Speed) has the strongest effect on hardness owed by factor *B* (Tool Rotational Speed) and factor *D* (Tool Angle). The Tool Pin Profile has the least effect on hardness. The mean response plot for hardness is presented in Fig. 7. The significance amongst the welding factors for output responses must also be calculated more precisely by using ANOVA analysis. The results of ANOVA analysis are given in Tab. 8. In this analysis, the consistency of process performance is recognized by greater R^2 value. Anticipated R^2 and adjusted R^2 show more accurate results. On the basis of ANOVA results, the estimated R^2 value of *HV*, R^2 = 99.66%. The R^2 value shows that its experiment sequence has a high degree of confidence in the system, It shows that welding speed (feed) is the most dominating factor of the process, showing an influence of 85.19% on *HV*.

Table 7 Response table for hardness

Level	Tool Pin Profile, *P*	Tool Rotational Speed, *N* / RPM	Welding Speed, *F* / mm/min	Tool Angle, θ / degree
1	61.56	59.17	67.00	61.33
2	61.56	62.67	61.67	61.17
3	--	62.83	56.00	62.17
Delta	0.00	3.67	11.00	1.00
Rank	4	2	1	3

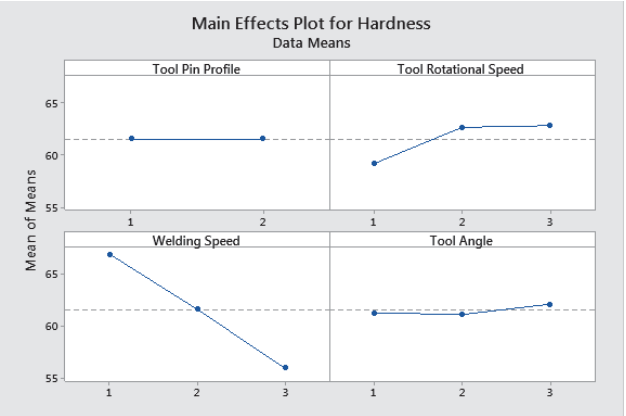

Figure 7 Main effects plot for hardness

Table 8 ANOVA results

Source	D*F*	Adj *SS*	Adj *MS*	*F*-Value	*P*-Value	% of Contribution
Ultimate Tensile Strength (*UTS*)						
Tool Pin Profile, *P*	1	0.99	0.99	0.01	0.914	0.022293
Tool rotational Speed, *N*	2	320.18	160.09	1.98	0.189	7.209784
Welding speed, *F*)	2	3232.04	1616.02	19.99	0	72.77878
Tool Angle, θ	2	79.47	39.73	0.49	0.626	1.789498
Error	10	808.23	80.82			18.19965
Total	17	4440.91				100
% of Elongation (*POE*)						
Tool Pin Profile, *P*	1	0.0050	0.00500	0.04	0.842	0.034225
Tool rotational Speed, *N*	2	0.9144	0.45722	3.81	0.059	6.258984
Welding speed, *F*	2	12.3211	6.16056	51.29	0.000	84.3368
Tool Angle, θ	2	0.1678	0.08389	0.70	0.520	1.148576
Error	10	1.2011	0.12011			8.221419
Total	17	14.6094				100
Micro Hardness (*HV*)						
Tool Pin Profile, *P*	1	1.785	0.8925	1.58	0.078	0.41879
Tool rotational Speed, *N*	2	51.444	25.722	39.91	0	12.0696
Welding speed, *F*	2	363.111	181.556	281.72	0	85.19173
Tool Angle, θ	2	3.444	1.722	2.67	0.118	0.808018
Error	10	6.444	0.644			1.511867
Total	17	426.228				100

3.4 Microscopy Analysis

The micro-photograph of the base metal taken through optical microscope is shown in Fig. 8. The grain boundaries are clear here with formation of large coarse grains [24]. Fig. 9 shows the micro image taken at heat affected zone adjacent to the processed region. When compared to the base metal micrograph, this micro image shows refined grains due to the inflow of heat from the core region.

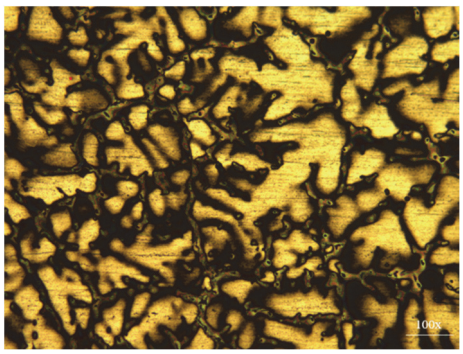

Figure 8 Micrograph of base metal (100x)

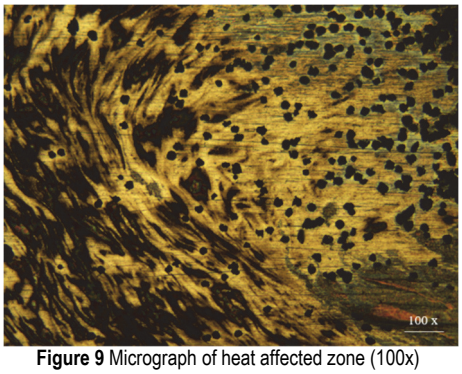

Figure 9 Micrograph of heat affected zone (100x)

The micrographs of the welded region are given below in Fig. 10 and Fig. 11. The micrographs clearly show the refinement of grains due to the effect of frictional heat produced and dynamic recrystallization under mechanical force [25]. The distribution of precipitate particles could also be seen in the micrographs [26]. The micrograph of Fig. 11 shows the isolation of the thermo mechanically influenced region from the primary stir region [27]. Though the refined grains tend to improve the mechanical properties, the defects that accumulate during the process become a cause for lower property values.

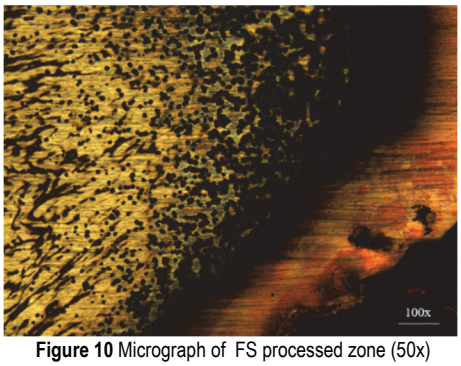

Figure 10 Micrograph of FS processed zone (50x)

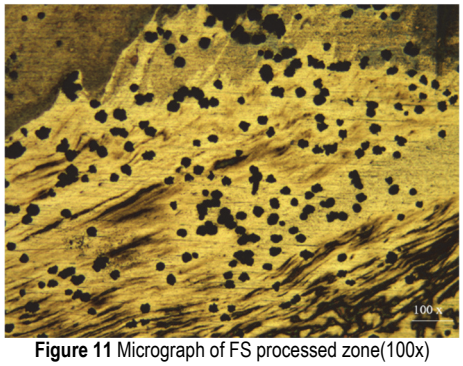

Figure 11 Micrograph of FS processed zone(100x)

4 MULTI-OBJECTIVE OPTIMIZATION USING TOPSIS TECHNIQUE

Hwang & Yoon [28] proposed the technique called TOPSIS. TOPSIS method solves the multi-response problem by comparing the different alternatives of the process. The principle involved in this technique is that it measures the compromise solution on the basis of how it is close and far to the ideal solution. The compromise solution is a hypothetical solution where all the parameters are directly related to the maximum attribute values in the database including the satisfying solutions. TOPSIS uses simple mathematical expressions with high computational efficiency to find ideal solutions to complex problems and hence it is widely used [29-30]. The procedural steps of TOPSIS technique can be explained in the following steps.

The TOPSIS technique transforms a multi-response system into a single optimized response. The TOPSIS begins with forming a decision matrix. The decision matrix (r_{ij}) is formulated through experimental results and presented in Tab. 5. The second step is defining the weight for each response. In step three, weighted normalized value of matrix is obtained by multiplying decision matrix with its preferred weights. This can be obtained with the help of Eq. (2).

$$r_{ij} = \frac{a_{ij}}{\sqrt{\sum_{i=1}^{m} a_{ij}^2}} \tag{1}$$

$a_{ij} = i$ th value of j th experimental run and r_{ij} = normalized value.

$$V_{ij} = W_i \cdot x \cdot r_{ij} \tag{2}$$

W_i = weight of a_{ij}.

In step four, S^+ (ideal best), S^- (ideal worst) are determined and separated by using Eq. (3) and Eq. (4.)

$$S_i^+ = \sqrt{\sum_{j=1}^{M} \left(v_{ij} - v_j^+\right)^2} \tag{3}$$

$$S_i^- = \sqrt{\sum_{j=1}^{M} \left(v_{ij} - v_j^-\right)^2} \tag{4}$$

In the final step, the closeness coefficient alternative (CC) is calculated by Eq. (5). After evaluation of CC, rank is given with respect to maximum CC value.

$$CC_I = \frac{S_i^-}{S_i^+ + S_i^-} \tag{5}$$

4.1 Numerical Computation of TOPSIS

The TOPSIS technique transforms a multi-response system into a single optimized response. The TOPSIS begins with forming a decision matrix. The decision matrix (r_{ij}) is formulated through experimental results and presented in Tab. 5. In step two, the normalized decision

matrix is obtained by normalizing the decision matrix. The weighted decision matrix is evaluated by multiplying with its criteria weights by using Eq. (2) and the values are presented in Tab. 9. The Ideal best (S^+) and the ideal worst (S^-) values were evaluated using Eq. 3 and Eq. 4 and the values are presented in Tab. 9.

Table 9 Normalization & Weighted Normalization

Expt. No.	Normalization			Weighted Normalization		
	UTS	*POE*	Avg *HV*	*UTS*	*POE*	Avg *HV*
1	0.2295	0.2598	0.2443	0.0918	0.0779	0.0733
2	0.2380	0.2297	0.2214	0.0952	0.0689	0.0664
3	0.2057	0.2033	0.2099	0.0823	0.0610	0.0630
4	0.2573	0.2673	0.2596	0.1029	0.0802	0.0779
5	0.2469	0.2485	0.2405	0.0988	0.0746	0.0721
6	0.2001	0.1732	0.2176	0.0800	0.0520	0.0653
7	0.2520	0.2749	0.2596	0.1008	0.0825	0.0779
8	0.2460	0.2410	0.2405	0.0984	0.0723	0.0721
9	0.2356	0.2071	0.2214	0.0943	0.0621	0.0664
10	0.2482	0.2561	0.2481	0.0993	0.0768	0.0744
11	0.2368	0.2259	0.2252	0.0947	0.0678	0.0676
12	0.2197	0.1657	0.2061	0.0879	0.0497	0.0618
13	0.2609	0.2786	0.2596	0.1044	0.0836	0.0779
14	0.2373	0.2297	0.2443	0.0949	0.0689	0.0733
15	0.1939	0.1958	0.2138	0.0776	0.0587	0.0641
16	0.2598	0.2673	0.2634	0.1039	0.0802	0.0790
17	0.2456	0.2673	0.2405	0.0983	0.0802	0.0721
18	0.2141	0.2071	0.2138	0.0857	0.0621	0.0641

Finally the value of closeness co-efficient (*CC*) is evaluated by using Eq. (5). Finally the ranking is done according to the closeness coefficient for each experimental run and presented in Tab. 10. The closeness co-efficient has been further optimized by Taguchi method.

Table 10 Separation measures and CCC

Expt. No.	S^+	S^-	*CCC*	RANK
1	0.01492	0.03364	0.6927	8
2	0.02140	0.02648	0.5530	10
3	0.03544	0.01229	0.2575	14
4	0.00387	0.04277	0.9171	3
5	0.01267	0.03425	0.7300	7
6	0.04220	0.00480	0.1021	16
7	0.00394	0.04323	0.9166	4
8	0.01451	0.03241	0.6907	18
9	0.02686	0.02131	0.4423	12
10	0.00964	0.03694	0.7930	6
11	0.02177	0.02558	0.5402	11
12	0.04142	0.01032	0.1994	15
13	0.00115	0.04609	0.9758	1
14	0.01838	0.02830	0.6062	9
15	0.03947	0.00932	0.1911	17
16	0.00342	0.04382	0.9276	2
17	0.00981	0.03827	0.7960	5
18	0.03213	0.01500	0.3183	13

On the basis of the *CCC* values obtained, the 18 experimental trials are ranked in such a way that ranking starts from the maximum to minimum with proximity coefficients and the order is:
13 > 16 > 4 > 7 > 17 > 10 > 5 > 1 > 8 > 14 > 2 > 11 > 9 > 18 > 3 > 12 > 15 > 6.

From Tab. 7, it can be seen that "trail no 13" has produced best results (highest *CCC* = 0.975, tool pin profile = threaded cylindrical, tool rotational speed = 1350 rpm, welding speed = 25 mm/min, tool tilt angle = 1.5°) providing the optimum set of FSP parameters from among the 18 trials conducted for achieving maximum performances simultaneously from all the input parameters involved.

4.1.1 Performance at Optimum Condition

The results obtained at optimum parametric combination are discussed below. The analysis revealed that experiment number 13 provided the optimum parametric conditions that include: Threaded cylidrical profile: tool rotational speed of 1200 rpm; feed of 25 mm/min; tool tilt angle of 1.5°. This particular combination produced the overall best results.

Tensile strength: Breakage of the specimens occurred at the processed zone in all the tests. This clearly indicates that the processed region is lesser in tensile strength than the parent metal. The maximum tensile strength obtained at the optimum combination is 206.35 MPa. This maximum value is 88.2% of the base alloy's tensile strength.

The minimum tensile strength obtained is 158.25 MPa (67.6% of base alloy) for the 6th experiment that has the parametric set of square profile, tool rotational speed of 1350 rpm. tool feed of 45 mm/min and tool tilt angle of 2°.

Percentage of elongation: The processed regions have shown lesser percentage of elongation compared to the base alloy. At optimum condition the percentage of elongation of the specimen is 7.4% which is 52.9% of the base alloy's value. The minimum value of percentage of elongation obtained in these experiments is 4.4% (31.4% of base alloy) for the 12th trial having the combination of threaded cylindrical profile, 1250 rpm, 45 mm/min and 15° angle. The defects causing inhomogeneity in the processed region could be attributed for such low values.

Hardness: For optimum condition, the hardness value obtained for the processed zone is *HV* 68 which is 79% of the base alloy's value. Though trial number 16 (ranked second in the order with threaded cylindrical profile, 1450 rpm, 25 mm/min and 2°) produces a hardness of *HV* 69, the tensile strength and percentage elongation values are lesser than 13th trail. However all the property values of trial 16 are very close to trial 13.

From the analysis of the results, it was noticed that some of the parametric combinations (experiment numbers: 16, 4, 7 & 10) show property values that are closer to the optimum condition values. It was also observed that in all these experiments the tool feed rate is the lowest of 25 mm/min and this factor is identified as the dominant factor of the FSP process among the given inputs.

4.2 Mean Response Table for CC

The significance of each FSP parameter can be shown through the response table and the graph of CC which are presented in Tab. 11 and Fig. 12 respectively. The response graph of CC reveals the variation in the response when the factor level increases from level 1 to level 3. On the basis of response graph and the response table, the optimal FSP parameter combination for FSP of AZ31B alloy is $P_2N_2F_1\theta_2$, by applying which maximum performance can be achieved. The results reveal that the tool rotational speed of 1450 rpm, the lowest feed of 25 mm/min and at a medium tool angle of 1.5° with threaded cylindrical tool pin profile gives maximum concrete solution.

Table 11 Mean response table for CC

Level	Tool Pin Profile	Tool Rotational Speed / RPM	Processing speed / mm/min	Tool Angle / degree
1	0.5891	0.5060	0.8705	0.5966
2	0.5942	0.5871	0.6527	0.6155
3	---	0.6819	0.2518	0.5629
Delta	0.0051	0.1760	0.6187	0.0527
Rank	4	2	1	3

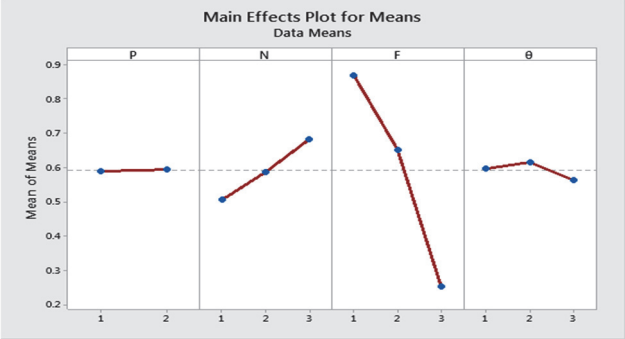

Figure 12 Response graph for *CC*

4.3 ANOVA Results

ANOVA is a technique used to evaluate the relative importance of all input factors on the response characteristics. The ANOVA value visibly indicates the contribution of each input factor on the process which is influenced by multiple factors.

Table 12 Analysis of variance for *CCC*

Source	D*F*	Adj *SS*	Adj *MS*	*F*-Value	*P*-Value	% Contribution
Tool Pin Profile, *P*	1	0.00012	0.000115	0.01	0.905	0.01
Tool Rotational Speed, *N*	2	0.09307	0.046536	6.06	0.019	6.84
Processing speed, *F*	2	1.18175	0.590873	76.90	0.000	86.87
Tool Angle, *θ*	2	0.00854	0.004271	0.56	0.590	0.63
Error	10	0.07684	0.007684			5.65
Total	17	1.36031				100.00

5 CONFIRMATION EXPERIMENT

Confirmation experiment (Tab. 13) is an important evidence to show the performance of optimized results. The tool rotational speed of 1350 rpm and the lowest welding speed of 25mm/min with tool angle of 1.5° using threaded cylindrical tool pin profile provides 206.15 MPa of *UTS*, 7.0% of *POE* and a *HV* of 70. The predicted *CCC* can be calculated using Eq. (6).

$$\hat{\eta} = \eta_m + \sum_{i=1}^{n} \left(\overline{\eta_i} - \eta_m \right) \tag{6}$$

where η_m is total mean of *CCC*, $\overline{\eta}$ is optimal level at each response.

Table 13 Confirmation test

	Initial parameters	Optimal Parameters	
		Prediction	Experiment
Setting level	$P_1N_1F_1\theta_1$	$P_2N_3F_1\theta_2$	$P_2N_3F_1\theta_2$
UTS	181.5	--	206.15
POE	6.9	--	7.0
HV	64	--	70
CCC	0.692	0.987	0.906
Improvement in *CCC* = 0.214			

6 CONCLUSIONS

- The AZ31B alloy plates were friction stir processed with copper tool by varying the tool profile and the parameters like tool rotational speed, tool feed and tool tilt angle. Experimental design of L_{18} mixed level, Anova for factor contribution and Topsis for optimization were used. The performance was analysed through tensile strength, percentage elongation and micro-hardness.
- The optimum set of parameters obtained through Topsis were: Tool pin profile of threaded cylindrical; Tool rotational speed of 1350 rpm: Tool feed of 25 mm/min and tool tilt angle of 1.5°.
- The property values obtained for the optimum set of parameters were: tensile strength of 206.35 MPa (88.2% of base metal value); percentage elongation of 7.4% (52.9% of base metal value) and vickers hardness value of *HV* 68 (79% of base metal value).
- Tool feed rate was found to be the most contributing factor of the FSP. Observation shows that the property values found to be closer to optimum values were obtained for the feed rate of 25 mm/min. in this experimentation.
- The optical micrographs showed refined grains at the FS processed zone. However the occurrence of defects in the course of processing affect the property values.

7 REFERENCES

[1] Balamurugan, K. G. & Mahadevan, K. (2013). Investigation on the changes effected by tool profile on mechanical and tribological properties of friction stir processed AZ31B magnesium alloy. *Journal of Manufacturing Processes, 15*(4), 659-665. https://doi.org/10.1016/j.jmapro.2013.04.001

[2] Hirsch, J. & Al-Samman, T. (2013). Superior light metals by texture engineering: Optimized aluminum and magnesium alloys for automotive applications. *Acta Materialia*, *61*(3), 818-843. https://doi.org/10.1016/j.actamat.2012.10.044

[3] Kumar, S. & Wu, C. S. (2017). Mg and its alloy scope, future perspectives and recent advancements in welding and processing. *Journal of Harbin Institute of Technology*, *24*, 1-37.

[4] Carcel, B., Sampedro, J., Ruescas, A., & Toneu, X. (2011). Corrosion and wear resistance improvement of magnesium alloys by laser cladding with Al-Si. *Physics Procedia*, *12*, 353-363. https://doi.org/10.1016/j.phpro.2011.03.045

[5] Mishra, R. S., De, P. S., & Kumar, N. (2014) Friction stir processing. In Friction stir welding and processing. *Springer, Cham*, 259-296. https://doi.org/10.1007/978-3-319-07043-8_9

[6] Babu, J., Anjaiah, M., & Mathew, A. (2018). Experimental studies on Friction stir processing of AZ31 Magnesium alloy. *Materials Today: Proceedings*, *5*(2), 4515-4522. https://doi.org/10.1016/j.matpr.2017.12.021

[7] Mishra, R. S. & Ma, Z. Y. (2005). Friction stir welding and processing. *Materials science and engineering: R: reports*, *50*(1-2), 1-78. https://doi.org/10.1016/j.mser.2005.07.001

[8] Kazemi, M. & Ghiasvand, A. (2021). Effect of cone angle of cylindrical pin in the SFSW and DFSW on mechanical properties of AA6061-T6 alloy. *International Journal of Mechanical and Materials Engineering,* (1), 1-13. https://doi.org/10.1186/s40712-021-00131-9

[9] Ghiasvand, A., Kazemi, M., Mahdipour Jalilian, M., & Ahmadi Rashid, H. (2020). Effects of tool offset, pin offset, and alloys position on maximum temperature in dissimilar FSW of AA6061 and AA5086. *International Journal of Mechanical and Materials Engineering*, *15*(1), 1-14. https://doi.org/10.1186/s40712-020-00118-y

[10] Ghiasvand, A., Kazemi, M., & Mahdipour Jalilian, M. (2021). Numerical investigation and prediction of grain size in different friction stir welding areas of AA6061 aluminum alloy. *Amirkabir Journal of Mechanical Engineering*, *53*(6), 20-20.

[11] Thomas, W. M. (1998). Friction stir welding and related friction process characteristics. *Proc. 7th International Conference Joints in Aluminium (INALCO'98)*, 1-18.

[12] Yang, J., Wang, D., Xiao, B. L., Ni, D. R., & Ma, Z. Y. (2013). Effects of rotation rates on microstructure, mechanical properties, and fracture behavior of friction stir-welded (FSW) AZ31 magnesium alloy. *Metallurgical and Materials Transactions A*, *44*(1), 517-530. https://doi.org/10.1007/s11661-012-1373-4

[13] Jayaraj, R. K., Malarvizhi, S., & Balasubramanian, V. (2017). Electrochemical corrosion behaviour of stir zone of friction stir welded dissimilar joints of AA6061 aluminium AZ31B magnesium alloys. *Transactions of Nonferrous Metals Society of China*, *27*(10), 2181-2192. https://doi.org/10.1016/S1003-6326(17)60244-9

[14] Dharmalingam, S., Lenin, K., & Krishnan, P. N. (2020). Comparative analysis of cylindrical thread and straight square profile pin on ultimate tensile strength of AA8011/AZ31B in friction stir butt welding. *Materials Today: Proceedings*, *21*, 523-526. https://doi.org/10.1016/j.matpr.2019.06.661

[15] Woo, W., Choo, H., Prime, M. B., Feng, Z., Clausen, B. (2008). Microstructure, texture and residual stress in a friction-stir-processed AZ31B magnesium alloy. *Acta materialia*, *56*(8), 1701-1711. https://doi.org/10.1016/j.actamat.2007.12.020

[16] Seifiyan, H., Sohi, M. H., Ansari, M., Ahmadkhaniha, D., & Saremi, M. (2019). Influence of friction stir processing conditions on corrosion behavior of AZ31B magnesium alloy. *Journal of Magnesium and Alloys*, *7*(4), 605-616. https://doi.org/10.1016/j.jma.2019.11.004

[17] Cao, X. & Jahazi, M. (2011). Effect of tool rotational speed and probe length on lap joint quality of a friction stir welded magnesium alloy. *Materials & Design*, *32*(1), 1-11. https://doi.org/10.1016/j.matdes.2010.06.048

[18] Rose, A. R., Manisekar, K., & Balasubramanian, V. (2011). Effect of axial force on microstructure and tensile properties of friction stir welded AZ61A magnesium alloy. *Transactions of Nonferrous Metals Society of China*, *21*(5), 974-984. https://doi.org/10.1016/S1003-6326(11)60809-1

[19] Rajakumar, S. & Balasubramanian, V. (2012). Multi-response optimization of friction-stir-welded AA1100 aluminum alloy joints. *Journal of Materials Engineering and Performance*, *21*(6), 809-822. https://doi.org/10.1007/s11665-011-9979-z

[20] Kadaganchi, R., Gankidi, M. R., & Gokhale, H. (2015). Optimization of process parameters of aluminum alloy AA 2014-T6 friction stir welds by response surface methodology. *Defence Technology*, *11*(3), 209-219. https://doi.org/10.1016/j.dt.2015.03.003

[21] Prasad, M. D. & Kumar Namala, K. (2018). Process parameters optimization in friction stir welding by ANOVA. *Materials Today: Proceedings*, *5*(2), 4824-4831. https://doi.org/10.1016/j.matpr.2017.12.057

[22] Kumar, S., Kumar, S. & Kumar, A. (2013). Optimization of process parameters for friction stir welding of joining A6061 and A6082 alloys by Taguchi method. *Proceedings of the Institution of Mechanical Engineers, Part C: Journal of Mechanical Engineering Science*, *227*(6), 1150-1163. https://doi.org/10.1177/0954406212459448

[23] Yuan, W., Mishra, R. S., Carlson, B., Verma, R., & Mishra, R. K. (2012). Material flow and microstructural evolution during friction stir spot welding of AZ31 magnesium alloy. *Materials Science and Engineering: A*, *543*, 200-209. https://doi.org/10.1016/j.msea.2012.02.075

[24] Akinlabi, E. T. & Mahamood, R. M. (2020). Solid-state welding: friction and friction stir welding processes. *Springer International Publishing*. https://doi.org/10.1007/978-3-030-37015-2

[25] Threadgill, P. L., Leonard, A. J., Shercliff, H. R., & Withers, P. J. (2009). Friction stir welding of aluminium alloys. *International Materials Reviews*, *54*(2), 49-93. https://doi.org/10.1179/174328009X411136

[26] Babu, J., Anjaiah, M., & Mathew, A. (2018). Experimental studies on Friction stir processing of AZ31 Magnesium alloy. *Materials Today: Proceedings*, *5*(2), 4515-4522. https://doi.org/10.1016/j.matpr.2017.12.021

[27] Pradeep, S., Sharma, S. K., & Pancholi, V. (2012). Microstructural and mechanical characterization of friction stir processed 5086 aluminum alloy. *Materials Science Forum.Trans Tech Publications Ltd.*, *710*, 253-257, https://doi.org/10.4028/www.scientific.net/MSF.710.253

[28] Hwang, C. L. & Yoon, K. (1981). Methods for multiple attribute decision making. Multiple attribute decision making. *Springer, Berlin, Heidelberg*, 58-191. https://doi.org/10.1007/978-3-642-48318-9_3

[29] Çelikbilek, Y. & Tüysüz, F. (2020). An in-depth review of theory of the TOPSIS method: An experimental analysis. *Journal of Management Analytics*, *7*(2), 281-300. https://doi.org/10.1080/23270012.2020.1748528

[30] Prabhu, S. R., Shettigar, A., Herbert, M., & Rao, S. (2018). Multi response optimization of friction stir welding process variables using TOPSIS approach. *IOP Conference Series: Materials Science and Engineering*, *376*(1), 012134. https://doi.org/10.1088/1757-899X/376/1/012134

Contact information:

Selvaraj MARAPPAN, Assistant Professor
(Corresponding Author)
Anna University,
Paavai Engineering College, Namakkal, Tamilnadu
E-mail: mselvarajpavai@gmail.com

Lenin KASIRAJAN, PhD, Professor
K Ramakrsihnan College of Engineering,
Samayapuram, Trichy, Tamilnadu
E-mail: leninnaga@yahoo.com

Vijayanand SHANMUGAM, PhD, Assistant Professor
Paavai Engineering College,
Namakkal, Tamilnadu
E-mail: msvijayanmechanical@gmail.com